ELSEVIER

Polymer 43 (2002) 899–907

polymer

www.elsevier.com/locate/polymer

The modelling of large deformations of pre-oriented polyethylene

J. Sweeney*, P. Caton-Rose, P.D. Coates

Department of Mechanical and Medical Engineering, IRC in Polymer Science and Technology, University of Bradford, Bradford BD7 1DP, UK

Received 4 June 2001; received in revised form 30 August 2001; accepted 12 September 2001

Abstract

High temperature reversion tests have revealed a state of pre-existing molecular orientation in extruded polyethylene sheet. This state is related to differences in stress-deformation behaviour when specimens of the sheet are stretched along different angles with respect to the extrusion direction. An established large deformation, rate-dependent constitutive equation has been developed to model this material, by incorporating the pre-orientation by the addition of a strained Gaussian network. The level of pre-orientation is deduced from the dimensional changes on shrinkage. The constitutive equation is incorporated into the finite element package ABAQUS, and the shapes and drawing forces of tensile specimens extended at various angles to the extrusion direction are modelled.

Keywords: Molecular orientation; Constitutive equation; Finite element

1. Introduction

Solid phase deformation processing is now a proven effective means of manufacture. Articles and engineering components are produced by this route with properties enhanced by molecular orientation. These processes involve the stretching, at elevated temperatures, of pre-formed polymer, often in the form of extruded sheet. When modelling the stretching process, some assumption is required as to the initial state of the material; often (e.g. Ref. [1]), it is reasonable to assume that the material is isotropic. However, it is known [2] that the properties of extruded sheet depend on the deformation and temperature history in a complex way, and that many of its mechanical properties are anisotropic. It is accepted [2] that a state of molecular orientation may exist in the extruded sheet.

We have observed cases in which the level of pre-orientation is high, and has significant effects in the subsequent deformation process. In this paper, we explore how to model the process while taking account of a general pre-existing state of orientation. This requires the development of a nonlinear constitutive law with the property of initial anisotropy, and its implementation within a finite element analysis. The resulting model is verified by comparison with the stretching at high temperature of specimens of extruded polyethylene sheet. The extruded sheet is pre-oriented, as established by observations of shrinkage, and the tensile axes of the specimens are at various angles with respect to this pre-orientation. The predictions of shapes and drawing forces are compared with experimental observations, the experimental strain fields being obtained using image capture.

2. Experimental

2.1. Material

The high density polyethylene material is characterised by weight and number averaged molecular weights $\bar{M}_W = 225,000$ and $\bar{M}_N = 24,000$, respectively, and by a short branch content of less than 1.5 butyls per 1000 carbons. The sheets used were made from this polymer with an addition of 2.5% by weight carbon black, as an aid to UV protection. Sheets were made by extrusion using a machine of single screw design, operating at a melt temperature of 190°C and outputting to an 8 mm feed. The extrudate was reduced to 4 mm thickness by flowing through a converging die, and then passed between rollers to a cooling stage. The final product was 3.9 mm thick.

2.2. Shrinkage

The level of pre-orientation of the extruded sheet was assessed by reversion tests. Specimens were heated in an oil bath at 150°C and the dimensional changes observed. Initially square specimens of side 100 mm with edges

* Corresponding author. Tel.: +44-1274-235456; fax: +44-1274-235425.

E-mail address: j.sweeney@bradford.ac.uk (J. Sweeney).

0032-3861/02/$ - see front matter
PII: S0032-3861(01)00624-3

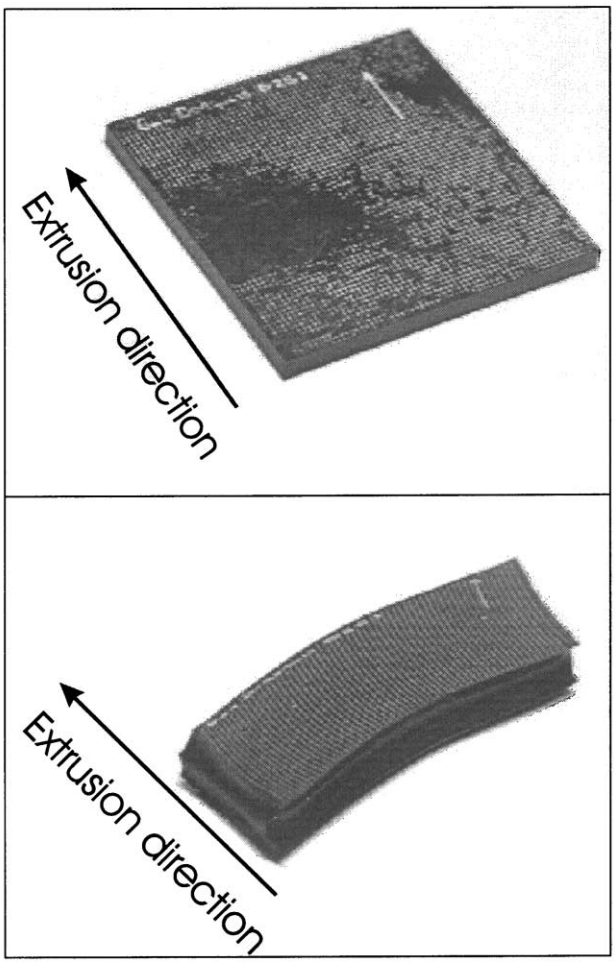

Fig. 1. Reversion tests for the extruded sheet, with the original specimen above and the reverted specimen below.

aligned with the extrusion direction, were used. After 15 min of immersion, the dimensions had ceased to change significantly, and the specimen was retrieved and its linear dimensions measured. A specimen in its initial and reverted states is shown in Fig. 1. The dimensional changes were large and easily measurable, leading to the conclusion that the sheet was pre-oriented to an extension ratio 3.1 along the extrusion direction, 0.75 normal to the extrusion direction in the plane of the sheet, and 0.43 through-thickness. The irregular shape of the reverted specimen suggests that the level of prestrain is not uniform throughout. It seems likely that the regions at the surfaces that cool quickly after extrusion will retain a higher level of orientation. However, at this stage this is difficult to quantify, and we proceed on the basis that the pre-orientation is uniform. The usefulness of this assumption will become apparent.

2.3. Tensile tests

Tensile specimens were made by punching regular arrays of holes in the extruded sheet, to give the required gauge geometry, and then cutting out the individual specimens.

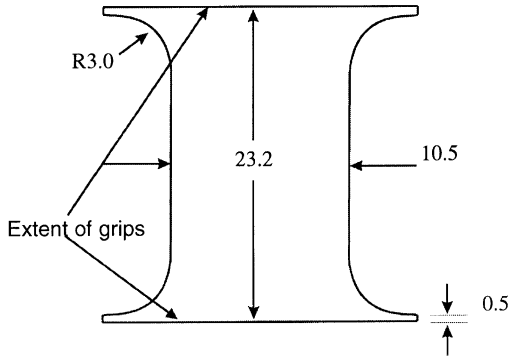

Fig. 2. Tensile specimen geometry. Dimensions in mm.

Thus, for the geometry illustrated in Fig. 2, the vertical surfaces bounding the gauge length and the adjacent circular arcs are the products of the punching process. The specimens were stretched in an environmental chamber in air at 110°C. The specimens were drawn at constant speeds, and the drawing force monitored, using an Instron testing machine. They were illuminated and their images captured through the window of the chamber using a digital camera. Strain profiles were then derived by analysis of the images, with the aid of lines printed on the specimen surfaces [3].

Specimens were produced with axes either along the extrusion direction normal to it or at 45°. Most tests were at the standard testing speed of 100 mm min^{-1}, though the slower speed of 20 mm min^{-1} was used to investigate rate dependence.

3. Constitutive equation

Arruda et al. [4] have developed a constitutive model in which the total plastic strain is subjected to a prestrain. In our approach, only a proportion of the polymer network is prestrained. Thus, the stress comprises two components. The greater of the two arises from the stretching of what we consider the 'main' network, governed by a nonlinear rate-dependent theory established previously which we term the 'sphere-in-box' model [5,6]. The minor component arises from the stretching of a Gaussian network (the 'subnetwork') that has been prestrained, with a pre-existing deformation gradient, uniform over the body. The prestrain is defined by a set of principal extension ratios and a director, corresponding to the initial direction of the greatest principal stretch.

The main network and the subnetwork differ physically from each other in that the former includes nonlinear viscoelastic effects while the latter is elastic. Stress in the subnetwork will therefore persist as long as it remains strained, while the stress in the main network will relax. An arrangement such as this is essential for the shrinkage to take place, since there are many fewer polymer chains in the subnetwork and yet it must, over time, overcome the resistance of the main network. We assume that, after

shrinkage has taken place, the stress in the main network has relaxed to zero, and so we may simply relate the observed shrinkage and the pre-orientation in the subnetwork.

At any integration point in the finite element model, there exists a deformation gradient tensor $\mathbf{G}$, defined as

$$\mathbf{G} = \left(\frac{\partial x_i}{\partial X_j} \right) \tag{1}$$

where the vectors in global 1–2–3 axes, (X_1, X_2, X_3) and (x_1, x_2, x_3), define material points in the undeformed and deformed states, respectively. To establish the main stress component, standard polar decomposition procedures [7] are applied. Forming the left Cauchy–Green strain measure, C eliminates rigid body rotations:

$$\mathbf{C} = \mathbf{G}\mathbf{G}^{\mathrm{T}} \tag{2}$$

Stresses for the sphere-in-box model are defined along principal directions. In the two-dimensional formulation adopted here, these are effectively defined by a single angle θ with the global 1 axis, with which the rotation R_θ is associated. The Cauchy–Green tensor in principal directions $\mathbf{C}_{\mathrm{p}}$ is then given by

$$\mathbf{C}_{\mathrm{p}} = R_\theta \mathbf{C} R_\theta^{\mathrm{T}} \tag{3}$$

From this tensor, we derive principal (I and II directions) extension ratios λ_{I} and λ_{II} in the plane, with the out-of-plane stretch λ_{III} defined via the incompressibility condition

$$\lambda_I \lambda_{II} \lambda_{III} = 1 \tag{4}$$

The significant feature of the sphere-in-box model [6] is that these principal stretches are used to derive effective principal stretches $\bar{\lambda}_{\mathrm{I}}$, $\bar{\lambda}_{\mathrm{II}}$, which reflect the strain concentrating effect of a hypothetical rigid sphere embedded in a cube of network material. At any time, the sphere radius is decreasing at a rate depending on the level of shear stress in the surrounding network, thus lowering the strain concentrating effect and introducing time dependence into the model. While the sphere may not be equated with any specific morphological features, the concept is motivated by the existence of stiff regions within the polymer that create strain concentration in the network; the rearrangement of microstructure on straining is represented by the shrinking of the sphere in response to shear stress. The network is assumed to be defined by the model of Ball et al. [8], which is elastic with the change in strain energy per unit volume W^{m} defined by

$$\frac{W^{\mathrm{m}}}{kT} = \frac{1}{2} N_{\mathrm{c}} \sum_{i=\mathrm{I}}^{\mathrm{III}} \bar{\lambda}_i^2 + \frac{1}{2} N_{\mathrm{s}} \sum_{i=\mathrm{I}}^{\mathrm{III}} \left(\frac{(1+\eta)\bar{\lambda}_i^2}{1+\eta\bar{\lambda}_i^2} + \ln\left(1+\eta\bar{\lambda}_i^2\right) \right) \tag{5}$$

where the superscript m denotes the main network. The physical quantities are k the Boltzmann constant, T the absolute temperature, N_{c} and N_{s} the number per unit volume of crosslinks and sliplinks, respectively and η a parameter governing the mobility of the sliplinks.

The sphere has a dimensionless radius R that evolves with time t according to the relation

$$\frac{\mathrm{d}R}{\mathrm{d}t} = -(R - R_\infty) A [\exp(B\tau) - 1] \tag{6}$$

The values of A, B and R_∞ are chosen so as to best characterise the observed material behaviour; R_∞ defines the lower limit of R, and its initial upper limit value R_{o} must also be specified. The process is driven by the quantity τ that is related to the maximum shear stress and defined by

$$\tau = \sigma^{\mathrm{m}}_{\max} - \sigma^{\mathrm{m}}_{\min}$$

where the quantities on the right are the greatest and smallest principal stresses in the main network. Thus, a total of seven parameters are required to define the sphere-in-box model.

As a result of the assumption of incompressibility (which applies by implication to the effective stretches) and the adoption of a plane stress formulation, principal stresses in the main network $\sigma^{\mathrm{m}}_{\mathrm{I}}$ and $\sigma^{\mathrm{m}}_{\mathrm{II}}$ are given by

$$\begin{aligned} \sigma^{\mathrm{m}}_{\mathrm{I}} &= \bar{\lambda}_{\mathrm{I}} \frac{\partial W^{\mathrm{m}}}{\partial \bar{\lambda}_{\mathrm{I}}} - \bar{\lambda}_{\mathrm{III}} \frac{\partial W^{\mathrm{m}}}{\partial \bar{\lambda}_{\mathrm{III}}} \\ \sigma^{\mathrm{m}}_{\mathrm{II}} &= \bar{\lambda}_{\mathrm{II}} \frac{\partial W^{\mathrm{m}}}{\partial \bar{\lambda}_{\mathrm{II}}} - \bar{\lambda}_{\mathrm{III}} \frac{\partial W^{\mathrm{m}}}{\partial \bar{\lambda}_{\mathrm{III}}} \end{aligned} \tag{7}$$

Finally, the principal stresses are transformed back through the angle θ to the global 1–2 axes to give the main network stresses σ^{m}_{11}, σ^{m}_{22} and σ^{m}_{12}.

We assume that the subnetwork is already stretched by a deformation gradient $\mathbf{S}$. When the deformation gradient $\mathbf{G}$ is applied, the stress response of this network is governed by the deformation gradient $\mathbf{G}^{\mathrm{s}} = \mathbf{G}\mathbf{S}$. Arruda et al. [4] used the same method to prestrain their plastic strain tensor. The deformation $\mathbf{G}^{\mathrm{s}}$ is analysed in the same way as $\mathbf{G}$ to reveal principal directions and principal extension ratios. Thus, as in Eq. (2), the Cauchy–Green tensor $\mathbf{C}^{\mathrm{s}}$ is generated:

$$\mathbf{C}^{\mathrm{s}} = \mathbf{G}^{\mathrm{s}} \mathbf{G}^{\mathrm{sT}} \tag{8}$$

The principal directions for this stretch are then found in the form of the angle ϕ between the principal I axis and global 1 axis, with which we associate the rotation R_ϕ. The principal Cauchy–Green tensor is then

$$\mathbf{C}^{\mathrm{s}}_{\mathrm{p}} = R_\phi \mathbf{C}^{\mathrm{s}} R_\phi^{\mathrm{T}} \tag{9}$$

from which the subnetwork principal extension ratios $\lambda^{\mathrm{s}}_{\mathrm{I}}$ and $\lambda^{\mathrm{s}}_{\mathrm{II}}$ are derived. We assume that the subnetwork deformation is incompressible, with the out-of-plane $\lambda^{\mathrm{s}}_{\mathrm{III}}$ stretch given by

$$\lambda^{\mathrm{s}}_{\mathrm{I}} \lambda^{\mathrm{s}}_{\mathrm{II}} \lambda^{\mathrm{s}}_{\mathrm{III}} = 1 \tag{10}$$

The stress in the subnetwork is assumed to arise from the stretching of a Gaussian network, with strain energy per unit volume W^{s} defined by

$$W^{\mathrm{s}} = N\left(\lambda^{\mathrm{s}2}_{\mathrm{I}} + \lambda^{\mathrm{s}2}_{\mathrm{II}} + \lambda^{\mathrm{s}2}_{\mathrm{III}} - 3\right) \tag{11}$$

Table 1
Main network parameters

N_c (MPa)	N_s (MPa)	η	R_o	R_∞	A (s^{-1})	B (MPa^{-1})
0.7	6.4	0.23	0.9	0.7	4.67×10^{-5}	0.71

The crosslink number N defines the stiffness of the subnetwork. Principal stresses are given by

$$\sigma_{\mathrm{I}}^{\mathrm{s}} = \frac{\partial W^{\mathrm{s}}}{\partial \lambda_{\mathrm{I}}^{\mathrm{s}}} - \frac{\partial W^{\mathrm{s}}}{\partial \lambda_{\mathrm{III}}^{\mathrm{s}}}$$
$$\sigma_{\mathrm{II}}^{\mathrm{s}} = \frac{\partial W^{\mathrm{s}}}{\partial \lambda_{\mathrm{II}}^{\mathrm{s}}} - \frac{\partial W^{\mathrm{s}}}{\partial \lambda_{\mathrm{III}}^{\mathrm{s}}} \tag{12}$$

The stresses must be transformed back to the global axis set through the angle ϕ to give the subnetwork stresses σ_{11}^{s}, σ_{22}^{s} and σ_{12}^{s}. To complete the subnetwork specification, the prestretch tensor **S** must be defined. This is assumed to be an incompressible deformation, so only two principal extension ratios, μ_{I} and μ_{II}, are required, together with a director angle α, defined as that between the global 1 axis and the extension μ_{I}. Thus these three parameters and N specify the subnetwork.

Finally, the total stress is given by the sum of stresses in the main network and the subnetwork:

$$\sigma_{11} = \sigma_{11}^{\mathrm{m}} + \sigma_{11}^{\mathrm{s}}$$
$$\sigma_{22} = \sigma_{22}^{\mathrm{m}} + \sigma_{22}^{\mathrm{s}} \tag{13}$$
$$\sigma_{12} = \sigma_{12}^{\mathrm{m}} + \sigma_{12}^{\mathrm{s}}$$

4. Numerical implementation

The constitutive equation outlined above was implemented using the package ABAQUS, via its UMAT user-defined material facility. An input of strain in the form of the deformation gradient **G** results in an output of total stress as finally given in Eq. (13). Also, there is the requirement for the Jacobian tensor that relates stress increments to strain increments. Its components are given by

$$\mathbf{J} = \begin{pmatrix} \frac{\partial \sigma_{11}}{\partial e_{11}} & \frac{\partial \sigma_{11}}{\partial e_{22}} & \frac{\partial \sigma_{11}}{\partial e_{12}} \\ \frac{\partial \sigma_{22}}{\partial e_{11}} & \frac{\partial \sigma_{22}}{\partial e_{22}} & \frac{\partial \sigma_{22}}{\partial e_{12}} \\ \frac{\partial \sigma_{12}}{\partial e_{11}} & \frac{\partial \sigma_{12}}{\partial e_{22}} & \frac{\partial \sigma_{12}}{\partial e_{12}} \end{pmatrix} \tag{14}$$

Table 2
Subnetwork parameters

N (MPa)	μ_{I}	μ_{II}
0.03	3.1	0.75

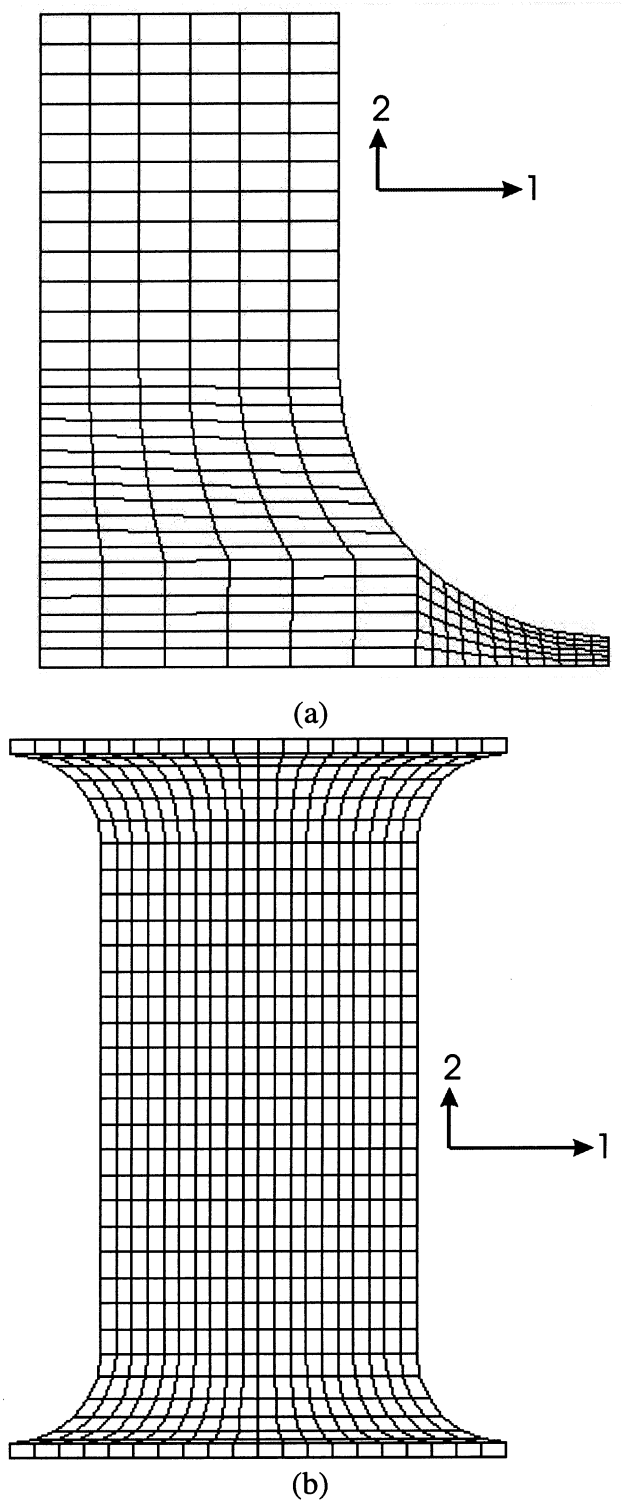

Fig. 3. Finite element meshes. (a) quarter model for symmetric cases and (b) full model for the director direction 45°.

where the e_{ij} are components of natural strain. The matrix **J** is asymmetric, and its nine components are generated numerically. For each deformation gradient **G**, four Cauchy–Green tensors are used. The first corresponds to

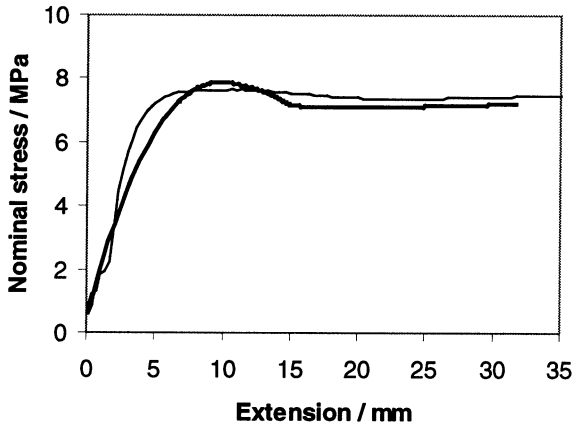

Fig. 4. Load–extension data for stretching along the extrusion direction: (—) observed, (—) modelled.

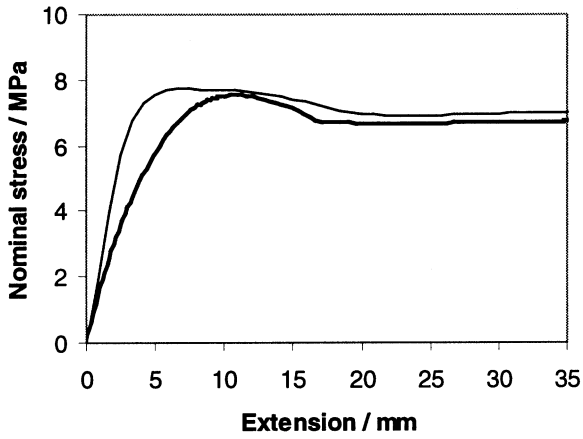

Fig. 6. Load–extension data for stretching at 45° to the extrusion direction: (—) observed, (—) modelled.

G and is given as **C** in Eq. (2), while the others are perturbations corresponding to small changes Δe_{11}, Δe_{22} and Δe_{12} in the strains e_{11}, e_{22} and e_{12}, respectively. The components of **J** are thus estimated by the differences $\Delta\sigma_{ij}/\Delta e_{ij}$ corresponding to the entries in **J** specified in Eq. (14).

5. Results and modelling

5.1. Parameter values

The values of the seven parameters required to define the main network are given in Table 1. We have arrived at them by a trial-and-error process aimed at producing the best fit to observed load–extension curves. This process is eased by the fact that some of the parameters have quite specific effects on the load–extension curves. The initial sphere radius R_o influences the deformation at which the initial load peak occurs (see Figs. 4–6). The ratio N_c/N_s controls the position of the load minimum. At large strains, the effect of the N_s term becomes negligible, and this aids the determination of the absolute value of N_c. The values of A and B control the strength of the rate dependence of the stress, and so they must correspond to the observed effect of different testing speeds on the peak stress. They also have a general effect on the predicted shapes.

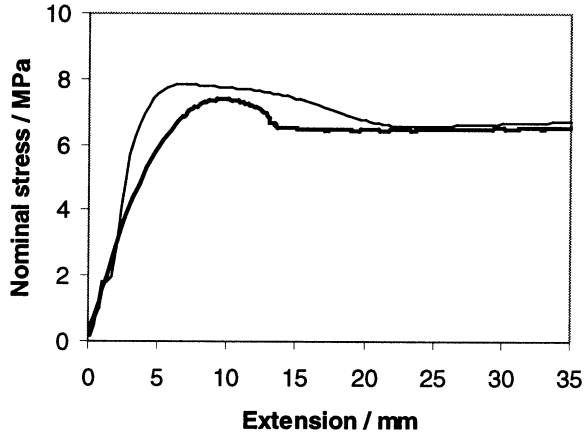

Fig. 5. Load–extension data for stretching normal to the extrusion direction: (—) observed, (—) modelled.

The subnetwork is characterised by three parameters. The crosslink number is determined from the difference in stress observed in tensile tests along different directions with respect to the extrusion direction, as described below in load–extension curves. The value of μ_I and μ_{II} are determined by shrinkage, as detailed above (Section 2.2), and are 3.1 and 0.75, respectively. The subnetwork parameters are summarised in Table 2.

5.2. Finite element models

We have subjected the geometry of Fig. 2 to two-dimensional plane stress analysis using the finite element package ABAQUS. Four-noded bilinear elements were used. The meshes are shown in Fig. 3. For director angles $\alpha = 0$ and $\alpha = \pi/2$, (α as defined in Section 3) the symmetry conditions are such that a quarter model is sufficient; this is shown in Fig. 3a. Otherwise, for $\alpha = \pi/4$, a full model is required, as shown in Fig. 3b. The numerical implementation has been described in Section 4.

5.3. Load–extension curves

The mesh of Fig. 3a is stretched along the extrusion axis ($\alpha = \pi/2$) to an extension equivalent to 32 mm of the complete specimen, at a speed equivalent to 100 mm min^{-1}. The predicted and observed load–extension curves are shown in Fig. 4, where load is plotted in the form of nominal stress. The model parameters give a good overall fit in quantitative terms, the main discrepancies being in the early part of the curve, where the peak load is predicted to occur at a somewhat later stage than the observed. A similar quality of fit is obtained for the lower speed of 20 mm min^{-1}, where the predicted peak nominal stress is lower with respect to the 100 mm min^{-1} test by 9%; this

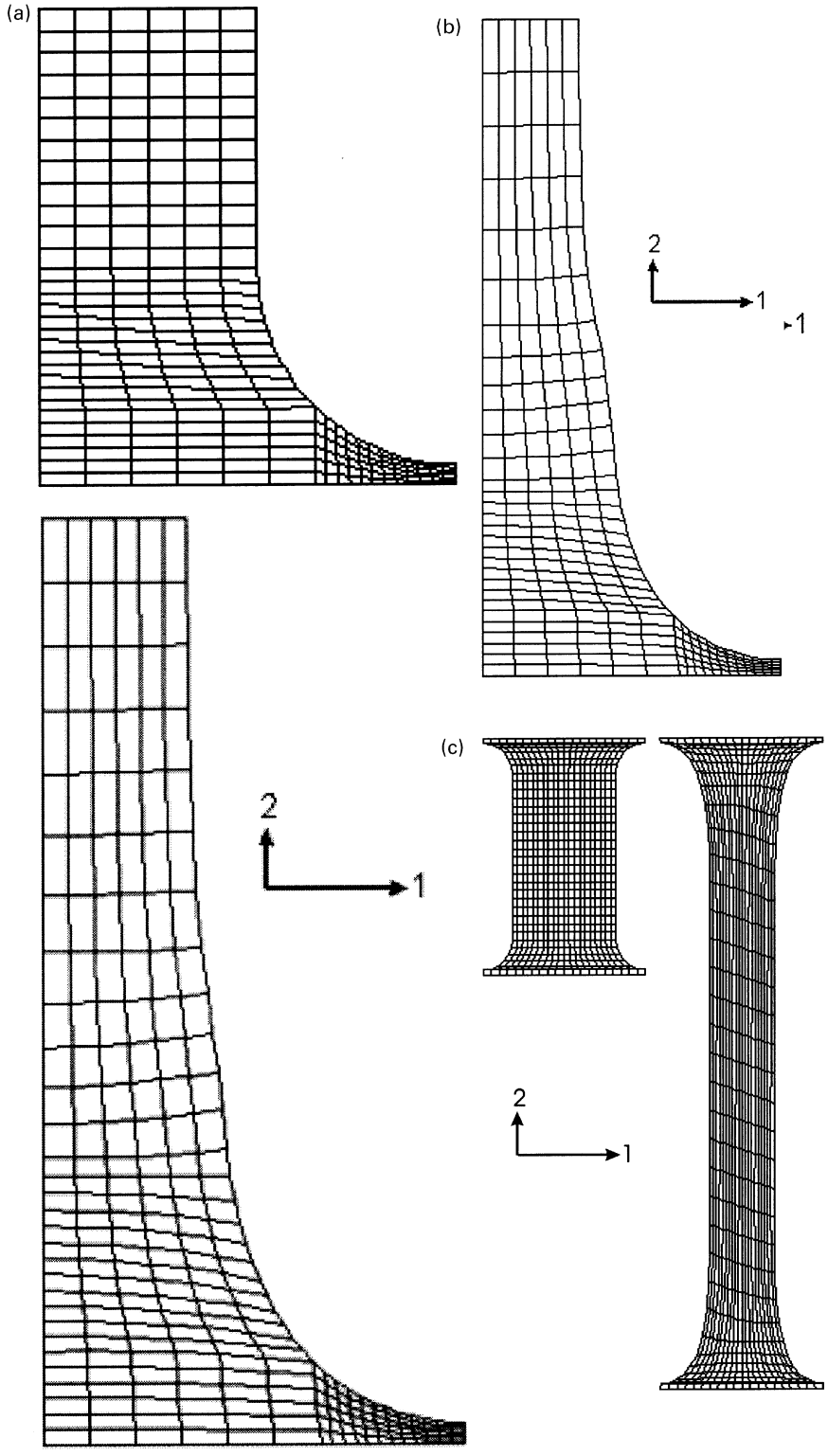

Fig. 7. Deformed meshes. (a) Along the extrusion direction, with undeformed mesh for comparison, extension 21 mm. (b) Normal to the extrusion direction, extension 21 mm. (c) 45° to the extrusion direction, with undeformed mesh for comparison, extension 32 mm.

should be compared with a lowering of the observed stress by 12%. The rate dependence of the stress is thus shown to be reasonably consistent with the predictions for strain rates in this range.

Similar comparisons are made for the case where stretching is normal to the extrusion direction ($\alpha = 0$). Fig. 5 shows the predictions of nominal stress. For both the observed and modelled curves, there is a greater drop in

stress after the peak in comparison with the above ($\alpha = \pi/2$) case. At extensions of 25 mm and more, there is good agreement for both $\alpha = 0$ and $\alpha = \pi/2$. The difference in stress between the two cases arises solely from the pre-oriented network, and the good predictions of the stress at large extension validates the chosen value of the crosslink number N for the subnetwork. It should be noted that the nominal stresses at these deformations differ significantly, with values of 7.4 MPa when $\alpha = \pi/2$ and 6.6 MPa when $\alpha = 0$.

Load–extension data for $\alpha = \pi/4$ are compared in Fig. 6. The validity of the prediction is similar to that which is obtained for the other director angles, again with good predictions of drawing stress at large extension.

5.4. Deformation fields

The models, stretched to deformations equivalent to 32 mm specimen extension at 100 mm min^{-1}, are shown in Fig. 7. It is clear that the necking shown in Fig. 7b, which is for the stretching normal to the extrusion axis, is more localised than that of Fig. 7a, where the stretching is along the extrusion direction. This conforms to observed behaviour. For the extension at 45° to the extrusion direction shown in Fig. 7c, the clear qualitative effect is that of the rotation of initially vertical lines of material points. This effect, a result of being relatively less extension along the stiff director, is borne out by the experimental observations.

Quantitative comparisons for deformations caused by the stretching along the extrusion direction are given in Fig. 8. Here the maximum axial extension ratio, occurring at the neck centre, is plotted. Initial and final extension ratios are predicted accurately, but there is an interim stage between extensions of 13 and 15 mm during which the deformation is predicted to develop too rapidly. At this stage the development of strain is controlled by the strain rate sensitivity of the stress $\partial\sigma_{11}/\partial\dot{e}_{11}$, where $\dot{e}_{11}$ is an appropriate measure of the strain rate [9]. The decrease in this quantity as the strain develops enables the strain rate to increase. The discrepancy between the observed and predicted localised strain, apparent in Fig. 8, is a measure of inaccuracy in the modelling of the decrease in strain rate sensitivity by the 'sphere-in-box' model. It should be noted that, if strain rate dependence were not included in the model, the increase in strain rate would begin at an earlier stage corresponding to an extension of 10 mm coinciding with the load peak shown in Fig. 4.

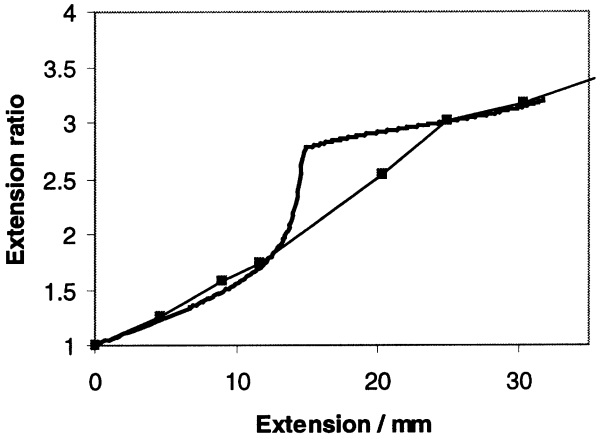

Fig. 8. Modelling of the development of axial strain at the specimen centre for drawing along the extrusion direction. (–■–) observed, (—) modelled.

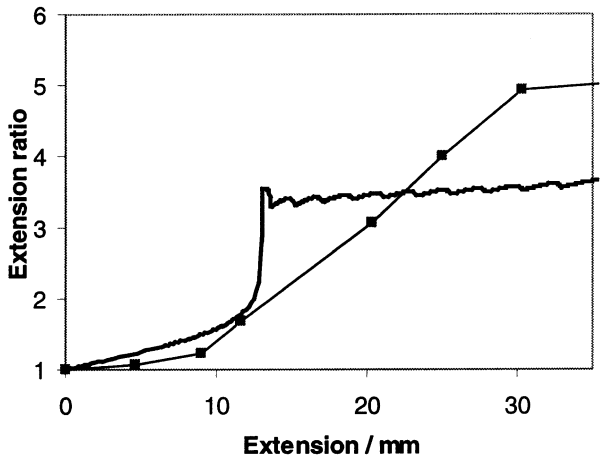

Fig. 9. Modelling of the development of axial strain at the specimen centre for drawing normal to the extrusion direction. (–■–) observed, (—) modelled.

For deformation normal to the extrusion direction, strains evolve more rapidly. This is reflected in the model predictions in Fig. 9 of maximum extension ratio. However, at a quantitative level the strain prediction shows a too-rapid development, beginning at an extension of 12 mm, which is suppressed at too low a value. The rapid increase in predicted strain is a similar effect to that for drawing along the extrusion direction, caused by poor modelling of the change in the strain rate sensitivity. After this process is complete, the strain rate settles to a low value, where the predicted level of strain is too low. This process is close to a

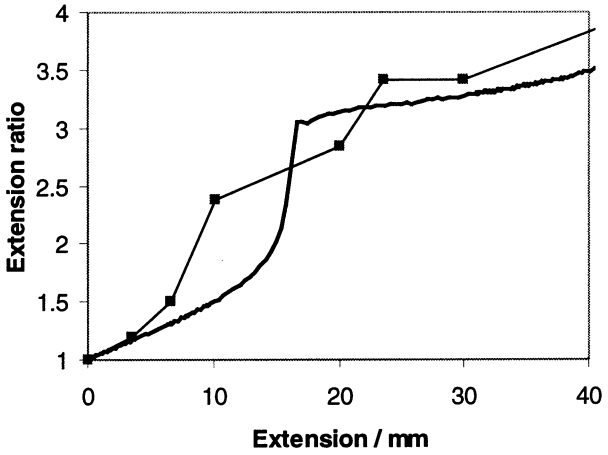

Fig. 10. Modelling of the development of axial strain at the specimen centre for drawing at 45° to the extrusion direction. (–■–) observed, (—) modelled.

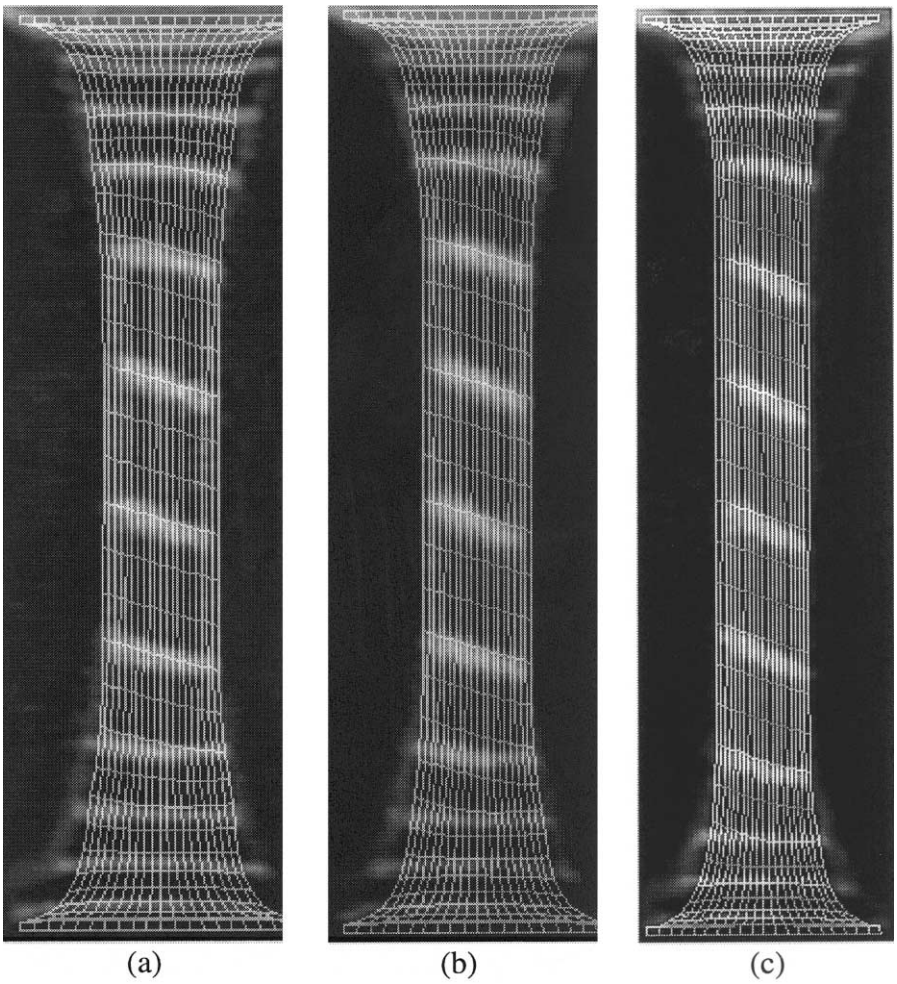

Fig. 11. Captured images of specimen markings overlayed onto distorted finite element meshes. (a) Extension 30 mm. (b) Extension 33 mm. (c) Extension 42 mm.

stable necking process, and corresponds to near constant values of nominal stress. The discrepancy in the observed and modelled strain levels in Fig. 9 corresponds to the difference in the specimen extension at which the observed and modelled stresses reach constant values, shown in Fig. 5. It is clear that at this stage of the process, the way in which the strain evolves is extremely sensitive to the small changes in the shapes of stress–strain curves.

For stretching at 45° to the extrusion axis, the observed and modelled maximum extension ratios are compared in Fig. 10. There is good agreement towards the end of the experiment, though this is preceded by significant discrepancies when both the observed and modelled strains are changing rapidly. Another important aspect of the deformation is the angle turned by lines of material in the gauge. The modelled rotation angles are compared with those observed in Figs. 11 and 12. Overlaying images of printed lines, initially normal to the extension direction, onto the distorted finite element mesh facilitates the comparison over the whole surface of the specimen. In Fig. 12, the angle at the centre of the specimen is plotted and compared with the prediction. The angle goes through a rapid change, which is predicted to occur at a somewhat earlier stage than the observed; the last observed angle is 19°, compared with the prediction of 16°. The finite element model can be seen to give a good representation of the observations.

6. Conclusions

The introduction of a pre-oriented Gaussian network component is an effective method of creating an initially anisotropic constitutive law. In the case discussed here, a Gaussian network is used, its material parameters — prestrain tensor and crosslink number — being evaluated by direct observations of shrinkage and of tensile testing along different material axes of an extruded HDPE sheet. The stress from this subnetwork is added to that arising from the main (initially isotropic) rate-dependent network. The resulting constitutive equation has been successfully implemented using the finite element package ABAQUS. This finite element analysis has been used to model the drawing forces

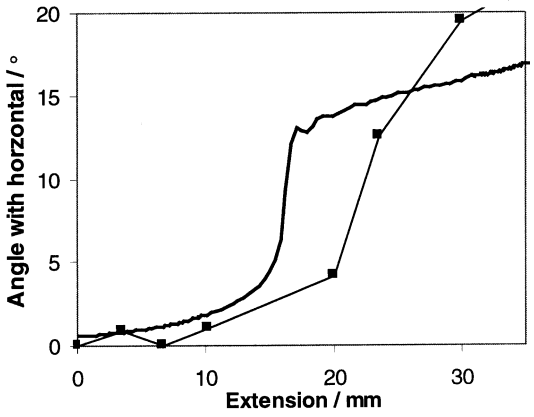

Fig. 12. Modelling of the development of the angle of initially horizontal lines of material at the specimen centre for drawing at 45° to the extrusion direction. (–■–) observed, (—) modelled.

and deformation fields that result from large tensile deformations of the sheet being applied along various axes relative to the extrusion direction. The experimental deformations have been quantified using image capture.

The existence of a pre-oriented state has significant effects on both the drawing forces and the drawn shapes, with necking of the specimens more severe for stretching normal to the extrusion direction. The finite element modelling reflects these effects well. In the case of stretching at 45° to the extrusion axis, there are gross qualitative effects on the deformation, which are again captured well by the finite element model.

Acknowledgements

We wish to thank Drs A.P. Unwin and R.A. Duckett, and Prof. I.M. Ward at the IRC in Polymer Science and Technology, University of Leeds, for stimulating discussions on pre-oriented polymer systems. Netlon Ltd, Blackburn, UK have provided extruded material and interesting discussions.

References

[1] Caton-Rose P, Sweeney J, Collins TLD, Coates PD. Plast Rubber Compos Process Appl 2000;29:51–8.
[2] Macauley NJ, Harkin-Jones EMA, Murphy WR. Polym Engng Sci 1998;38:662–73.
[3] Haynes AR, Coates PD. J Mater Sci 1996;31:1843–55.
[4] Arruda EM, Boyce MC, Quintus-Bosz H. Int J Plasticity 1993;9:783–811.
[5] Sweeney J, Collins TLD, Coates PD, Duckett RA, Ward IM. Int J Plasticity 2001, in press.
[6] Sweeney J, Collins TLD, Coates PD, Duckett RA. J Appl Polym Sci 1999;72:563–75.
[7] Bonet J, Wood RD. Nonlinear continuum mechanics for finite element analysis. Cambridge: Cambridge University Press, 1997.
[8] Ball RC, Doi M, Edwards SF, Warner M. Polymer 1981;22:1010–8.
[9] Sweeney J, Shirataki H, Unwin AP, Ward IM. J Appl Polym Sci 1999;74:3331–41.